Ultralow-Noise Chopper Amplifier With Low Input Charge Injection

Dietmar Drung and Jan-Hendrik Storm

Abstract—A chopper amplifier is presented that achieves an ultralow voltage noise of $0.73 \text{ nV}/\sqrt{\text{Hz}}$ down to a few millihertz. Excess white and $1/f$ current noise was observed, which increases with the chopping frequency. At the lowest chopping frequency of 570 Hz, a noise level of $40 \text{ fA}/\sqrt{\text{Hz}}$ with a $1/f$ corner at 3 mHz is obtained, corresponding to a noise temperature around 1 K at the optimum source impedance of 18 kΩ. Special care was taken to compensate the effect of switching spikes in the input chopper, resulting in a low charge injection into the signal source. The amplifier has a fixed gain of 1000. Postamplification and postfiltering with a wide range of settings, as well as optical output isolation based on a highly linear voltage-to-frequency converter, make the instrument well suited for demanding applications in metrology.

Index Terms—Chopper amplifier, input charge injection, nanovoltmeter, optical isolation, voltage–frequency conversion.

I. INTRODUCTION

VERY low uncertainty resistance bridges based on cryogenic current comparators (CCCs) are used in many national metrology institutes worldwide. They require a null detector with very low equivalent input voltage and current-noise levels. Commercial instruments like the nanovoltmeter N11 from EM Electronics [1] are widely used for this purpose. The N11 achieves the required ultralow noise performance but is limited to a bandwidth below about 1 Hz, exhibits a relatively low input impedance at high frequencies, and (under some circumstances) disturbs the superconducting quantum interference device (SQUID) used in the CCC due to input charge injection.

In this paper, we present a newly developed chopper amplifier that matches the voltage noise performance of the N11 but has significantly improved current noise, measurement bandwidth, high-frequency input impedance, and input charge injection [2]. The amplifier is used as a null meter in our new CCC-based resistance bridge [3] and allows us, for the first time, to investigate the settling behavior of the bridge voltage [4]. The design and the performance of the new amplifier are presented in Sections II and III. Postamplification and postfiltering of the output signal are discussed in Section IV. A newly developed voltage-to-frequency V/f converter for
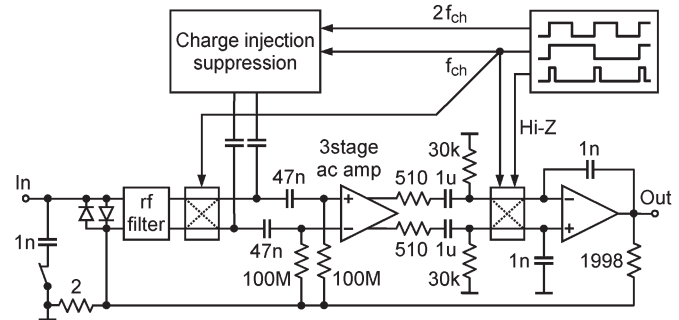
Fig. 1. Basic circuit diagram of the chopper amplifier. Details are omitted for clarity.

optical output isolation is described in Section V. This paper is finished with two application examples (see Section VI) and a brief conclusion (see Section VII).

II. AMPLIFIER DESIGN

The basic building blocks of the chopper amplifier are depicted in Fig. 1. After passing a radio-frequency (RF) filter, the direct-current (dc) input is converted into a square wave by a chopper circuit [5] that is realized using high-speed complementary metal–oxide–semiconductor (CMOS) switches with a very low on-resistance of $\approx 3.5 \ \Omega$. Controlled by clock f_{ch}, the signal is connected to the input of an alternating-current (ac) coupled amplifier either directly (solid lines in the chopper box) or with reversed polarity (dotted lines). The amplifier involves three stages built with discrete junction field-effect transistors, bipolar RF transistors, and high-speed operational amplifiers. It has differential inputs and outputs, a nominal gain of 2000, a gain-bandwidth product of about 50 GHz, and a low-frequency rolloff at ≈ 300 Hz. A 34-mHz-high pass at the amplifier input eliminates the effect of the input bias current drift, and a 310-Hz-high pass at the amplifier output suppresses the low-frequency voltage noise.

The amplifier-output square wave is synchronously rectified by another chopper, integrated using an operational amplifier, and fed back to the input to provide an overall gain of 1000. The operational amplifier has a high open-loop gain of 10^6, which results in high stability and linearity of the overall gain.

The output chopper is set into a high-impedance (hi-Z) state for 230 ns after each clock edge. This "guard band" reduces the effect of switching transients [5]. A special charge-injection suppression circuit feeds an adjustable amount of compensation charge into the amplifier input at each clock edge. This strongly reduces the amplitude of switching spikes

in the input chopper. The RF filter at the chopper input further suppresses the switching spikes and makes the amplifier less sensitive to electromagnetic interference (EMI). An optional 1-nF capacitor across the input improves the filtering of spikes and enhances the EMI immunity. The total input capacitance is 160 pF without the 1-nF capacitor. Note that only 50 pF is caused by the amplifier alone.

The amplifier is housed in a hermetically closed metal box. The supply voltage is ± 5 V, and the total quiescent current is about 65 mA. The power is taken from two 6-V 3.5-Ah lead batteries and is stabilized by low-noise ± 5-V voltage regulators. This enables continuous battery operation over long periods. A special charging unit was developed, which is based on a home-made dc–dc converter with a high switching frequency of about 180 kHz. A ferrite ring core with an outer diameter of only 10 mm is used for the transformer in order to minimize capacitive coupling. The setup is very compact compared with other low-noise highly isolated power supplies [6], [7]. In spite of the small transformer size, a maximum charging current of more than 0.5 A can be delivered. A very high electrical isolation is achieved by using a polytetrafluoroethylene-insulated wire for the transformer primary. Therefore, the mains operation is possible even in sensitive measurements with virtually no distortion or leakage.

III. AMPLIFIER PERFORMANCE

The timer circuit allows a variation of the chopping frequency between 570 Hz and 177 kHz. The chopping frequencies are approximately equally spaced in a log scale with an increment factor of $\approx \sqrt{10}$. The lowest chopping frequencies of 570 Hz and 1.77 kHz are harmonically unrelated to 50 and 60 Hz, thus avoiding potential problems caused by mains interference. For measuring the voltage noise, we shorted the amplifier input directly on the printed-circuit board. A very wide minimum of 0.71 nV/$\sqrt{\text{Hz}}$ was found for chopping frequencies around 5.7 kHz. The root-mean-square (RMS) voltage noise increased by only 3% when changing the chopping frequency to 570 Hz or 57 kHz. The noise was white down to a few millihertz (cf. Fig. 2). At the highest chopping frequency of 177 kHz, a noise level of 0.77 nV/$\sqrt{\text{Hz}}$ was measured.

The low-frequency noise spectra in Fig. 2 were averaged for at least 12 h. During these overnight measurements, we observed a drift of typically 1 nV/h. This was caused in part by a somewhat unfavorable placement of the power supply in the amplifier box, which leads to temperature gradients on the amplifier board depending on the charging condition of the batteries. This thermal interaction will be minimized in the final amplifier version. The unadjusted input offset voltage was well below 1 μV. For the noise measurements presented here, it was not necessary to adjust the offset to zero.

The current noise was investigated in the aforementioned range of chopping frequencies f_{ch}. We found three characteristic noise components: a white "base" noise of about 20 fA/$\sqrt{\text{Hz}}$, which is independent of f_{ch}, plus white and $1/f$ excess noises depending on f_{ch}. The white chopping noise (≈ 45 fA/$\sqrt{\text{Hz}}$ at $f_{ch} = 1$ kHz) scales with the square root of the chopping frequency, i.e., $\sqrt{S_I} \propto \sqrt{f_{ch}}$. In contrast, the $1/f$
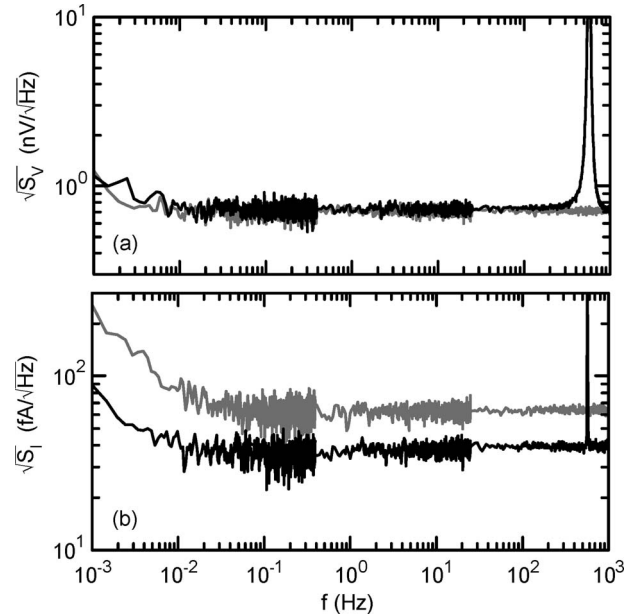

Fig. 2. (a) Voltage and (b) current noise spectra of the amplifier for chopping frequencies of (black lines) 570 Hz and (gray lines) 1.77 kHz. The current noise was measured with a 10-MΩ resistor across the input. The low-pass response caused by this resistor and the 1.16-nF input capacitance, as well as the Nyquist noise in the 10-MΩ resistor (≈ 40 fA/$\sqrt{\text{Hz}}$), was considered in the data analysis.
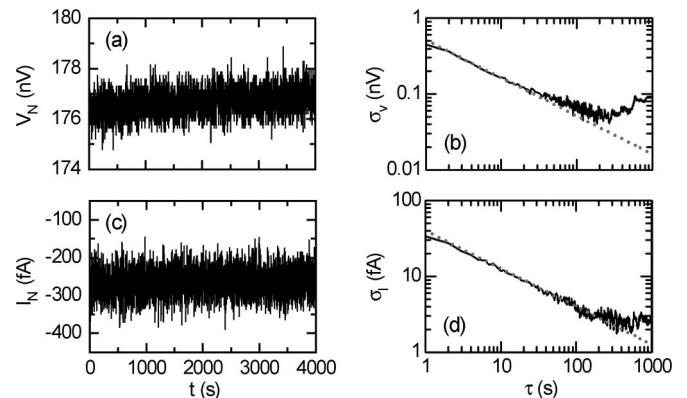

Fig. 3. Input-referred low-frequency performance of the amplifier for a chopping frequency of 570 Hz. Time traces (a) with a shorted input and (c) with a 10 MΩ resistor across the input were acquired using an HP35667A signal analyzer with a filter bandwidth of 0.4 Hz. The corresponding Allan deviations σ_V and σ_I are shown on the right side in (b) and (d) as a function of the measurement time τ. (Dotted lines) Calculated from the white noise levels of the noise spectra in Fig. 2 ($\sigma \propto 1/\sqrt{\tau}$). Note that the Nyquist noise from the 10-MΩ resistor (≈ 40 fA/$\sqrt{\text{Hz}}$) is included in the current-noise data.

chopping noise (≈ 3.5 fA/$\sqrt{\text{Hz}}$ at $f = 1$ Hz and $f_{ch} = 1$ kHz) linearly scales with the chopping frequency, i.e., $\sqrt{S_I} \propto f_{ch}$. Note that $1/f$ means $\sqrt{S_I} \propto 1/\sqrt{f}$. The total current noise for a selected chopping frequency can be predicted by building the RMS sum of the three noise components. For example, for the highest chopping frequency of 177 kHz, a white noise of 0.6 pA/$\sqrt{\text{Hz}}$ and a $1/f$ corner of about 1 Hz are predicted in good agreement with the measured result.

Fig. 3 shows low-frequency time traces and the corresponding Allan deviations for a chopping frequency of 570 Hz. The Allan variance is a convenient alternative to the power
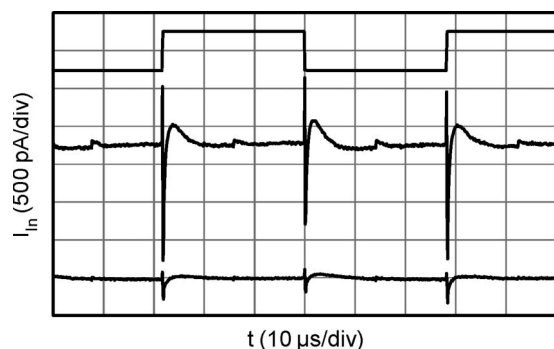
Fig. 4. Input charge injection of the chopper amplifier measured with a 10-kΩ source resistance. (Top to bottom) Chopper clock, input current without optional 1 nF across the input, and input current with 1 nF. The traces are vertically shifted for clarity.
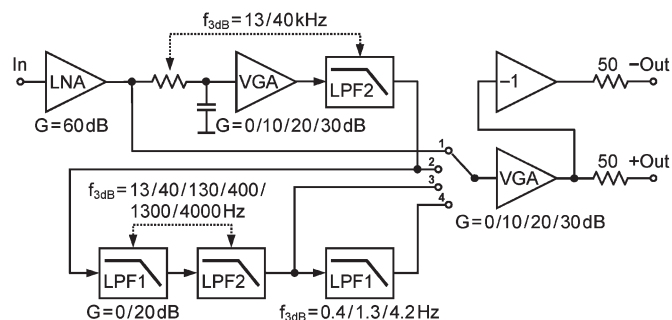

Fig. 5. Concept of postamplification and postfiltering, allowing a wide range of overall gain and measurement bandwidth. The chopper amplifier (LNA) is followed by amplification stages (VGA) and first/second-order low-pass filter stages (LPF1/LPF2). The latter are combined to provide third-order low-pass responses with the quoted 3-dB cutoff frequencies. The filter stages have unity gain unless otherwise noted.

spectral density for the description of noise effects [8]. As an example, for a white voltage noise with a spectral density S_V, the corresponding Allan deviation $\sigma_V = (S_V/2\tau)^{1/2}$, where τ is the measurement time. Taking the white noise levels of 0.73 nV/$\sqrt{\text{Hz}}$ and 40 fA/$\sqrt{\text{Hz}}$ from the spectra in Fig. 2, we predict Allan deviations of 163 pV and 9 fA, respectively, for a measurement time of 10 s. The latter increases to 12.7 fA when including the Nyquist noise in the 10-MΩ resistor connected across the amplifier input for performing the current-noise measurements. The Allan deviations predicted from the white noise levels (dotted lines in Fig. 3) are in good agreement with the measured results over a wide range of measurement times τ. Deviations at short measurement times are due to the input filter of the signal analyzer, whereas those at long measurement times are caused by the $1/f$ noise and (in the case of the voltage noise) by drift effects.

For all current-noise measurements, a 10-MΩ resistor was connected across the amplifier input. To ensure that the results were not affected by the amplifier-input impedance, we estimated it by applying a test signal to the input either directly or via a 1-GΩ resistor. The corresponding change in the output signal was of the order of 1%, implying a sufficiently high input impedance of about 100 GΩ.

The input charge injection was investigated by measuring the voltage at a 10-kΩ resistor connected to the amplifier input. As shown in Fig. 4, the optional 1-nF filter capacitor at the amplifier input strongly suppresses the residual switching spikes. Note that the net input bias current was adjusted to zero via the charge-injection suppression circuit.

For comparison, we measured the noise and the input charge injection of one of our N11 nanovoltmeters [1], which runs at a chopping frequency of 290 Hz. The voltage noise of about 0.7 nV/$\sqrt{\text{Hz}}$ is comparable with that of the presented chopper amplifier, but the current noise of about 0.5 pA/$\sqrt{\text{Hz}}$ is considerably higher for similar chopping frequencies. The N11 produces high-frequency current spikes of about 10 nA into a 10-kΩ source corresponding to the 8-fC charge injection. In contrast, the input spikes of our chopper amplifier are much smaller (amplitude of about 300 pA and 1 fC with 1 nF across the input). Thus, we conclude that the new amplifier is well suited for precision measurements that require an ultralow-noise level and a low charge injection into the signal source.

IV. POSTAMPLIFICATION AND POSTFILTERING

The chopper amplifier has a fixed gain of 1000 and a small-signal bandwidth of over 300 kHz. The corresponding input voltage range is ±3 mV. Due to the chopping process, switching spikes are superimposed to the amplifier output signal. Therefore, appropriate low-pass filters and postamplification stages with selectable gain are mandatory for using the amplifier in demanding metrology applications.

The order of the various postfilter and postamplification stages is crucial. One has to ensure that neither the input-referred amplifier noise level is degraded nor any of the filter/amplification stages is overdriven or slew-rate limited. For example, if the power-line interference exceeds the dynamic range of an amplifier stage followed by a power-line filter, the filter output might appear "clean," although it is strongly distorted by the internal overload. Furthermore, filter stages with a low cutoff frequency imply long time constants. Dielectric absorption in the filter capacitors leads to a slowly decaying distortion after a signal step, e.g., after each current reversal in a CCC-based resistance comparison similar to the effect in the long cables of the setup [4]. This parasitic signal is further increased by the following amplification stages. Therefore, filter stages with long time constants should be placed as close as possible to the end of the amplification chain in order to improve the recovery time after a strong overload.

Fig. 5 shows our concept of postamplification and postfiltering, which considers all these issues. The overall gain G can be varied in 10-dB steps between 60 and 140 dB. The range of cutoff frequencies covers five orders of magnitude, i.e., 0.4 Hz to 40 kHz in steps of about 10 dB. The cutoff frequency can be selected according to the measurement requirements and the chopping frequency (cf. the pronounced chopping noise peak in the voltage noise spectrum in Fig. 2). An inverted output is realized to increase the flexibility. This allows, for example, the realization of a low-noise amplifier (LNA) input resistance $R_F/(G+1)$ by simply feeding back the inverted amplifier output to the input via resistor R_F. It has been recently suggested to read out a series array of transition-edge sensors with the presented chopper amplifier by using this feedback scheme [9].

The unfiltered amplifier output is available in position 1 of the selection switch in Fig. 5. The variable gain amplifier

(VGA) after the switch provides 0–30 dB of extra gain. In switch position 2, a high-frequency filter and an extra gain stage can be activated. This filter consists of a passive RC low pass that is directly placed at the chopper amplifier output to effectively suppress the switching spikes before the signal is passed to the gain stage. Together with an active second-order low pass after the gain stage, an overall third-order low-pass response with a selectable 3-dB cutoff frequency of 13 or 40 kHz is obtained. This high-frequency filter is used as a prefilter for the following filter stages when the switch is in position 3. With the lowest cutoff frequency of 13 Hz, the 50-Hz power-line interference is reduced to about 4%. Finally, in switch position 4, an extra low-frequency first-order low pass can be selected to further reduce the wideband noise. Note that the 4.2-Hz first-order low pass yields an overall 4-Hz cutoff frequency when being combined with the preceding 13-Hz third-order filter.

V. OPTICAL OUTPUT ISOLATION

An optically isolated amplifier output is desirable to avoid ground loops in complex measurement setups. For some applications, it is even a must, e.g., in CCC-based resistance bridges where leakage currents have to be avoided to achieve high precision [10]. For our amplifier, we have realized an optical output isolation based on the voltage-to-frequency V/f conversion. We chose a relatively high output-frequency range of 1–2 MHz to obtain a good dynamic behavior. The input voltage range of ± 3 V is converted into a frequency range of ± 0.5 MHz centered around 1.5 MHz. Each hertz change in the frequency output corresponds to a relative change of 1×10^{-6} of the full-scale (FS) output.

Commercially available monolithic V/f converters did not provide sufficiently low noise and high speed for our new CCC-based resistance bridge [3], particularly when using them in the external feedback loop stabilizing the flux through the SQUID. Therefore, in order to achieve the lowest possible noise and a high bandwidth, we developed a homemade V/f converter. It basically involves a high-speed comparator and a precise 180-pF capacitor with a fast CMOS switch in parallel. The capacitor is relatively slowly charged until a certain threshold voltage is reached. At this time, the comparator output state changes and causes the switch to short the capacitor for about 26 ns. After this discharge period, the next cycle starts with charging the capacitor again. The charging current and, thus, the charging time is controlled by the analog input voltage such that a linear voltage-to-frequency conversion is obtained. For our prototype, we measured a nonlinearity (i.e., maximum deviation from a linear transfer function) of about $\pm 0.1\%$. A second-order low-pass filter at the input of the V/f converter suppresses wideband noise.

The achieved nonlinearity is not sufficient for demanding metrology applications. Therefore, we linearized the transfer function of the V/f converter by using a servo loop with a highly linear f/V converter (see Fig. 6). Below the unity-gain frequency of about 13 kHz, the servo loop provides gain, and the overall behavior (noise and linearity) is determined by the performance of the f/V converter alone.
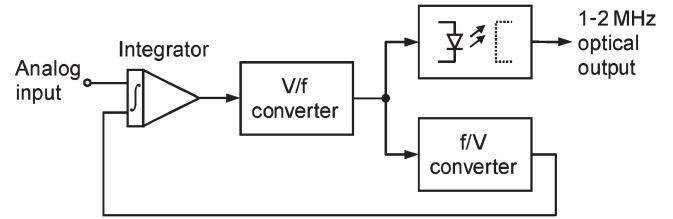

Fig. 6. Scheme of the V/f converter for optical isolation. The V/f converter response is linearized by using a servo loop involving a highly linear f/V converter. The frequency output can be back converted into an analog voltage with a f/V converter identical to the one in the servo loop. Alternatively, a counter may be used to convert the frequency output directly into a digital data stream.

At each positive slope of the input-pulse sequence, a well-defined output pulse of 4.5-V amplitude and 420-ns duration is generated in the f/V converter. The average voltage of this precision output-pulse sequence linearly scales with the pulse frequency provided that the pulse area (the product of the pulse amplitude and duration) does not depend on the pulse frequency. This can be achieved to a high degree by a careful circuit design. The output of the precision pulse generator is filtered with a fifth-order low pass such that the remaining ac amplitude disappears in the noise band. The white RMS noise level at the output of the f/V converter scales with the square root of its input frequency, i.e., $\sqrt{S_V} \propto \sqrt{f_{\text{In}}}$. In contrast, the $1/f$ noise contribution linearly scales with the input frequency, i.e., $\sqrt{S_V} \propto f_{\text{In}}$. At the center frequency of 1.5 MHz, a white noise level of 0.8 $\mu V/\sqrt{Hz}$ and a $1/f$ noise contribution of 1.8 $\mu V/\sqrt{Hz}$ at 1 Hz were obtained for the selected output voltage range of ± 3 V.

The dynamic behavior of the linearized V/f converter was investigated by applying a test signal to the analog input and measuring the voltage at the output of the f/V converter (cf. Fig. 6). We found a small-signal bandwidth of about 40 kHz and a circuit delay of 9 μs, measured between the 50% points of the input and the output.

The test circuit of the linearized V/f converter showed a good linearity but an insufficient thermal stability of the transfer coefficient. This was caused by the temperature dependence of the critical components in the f/V converter (mainly timing capacitor and comparator delay), which affects the pulse area. In order to improve the thermal stability, we added a reference f/V converter, which is driven by a quartz clock and controls the main f/V converter in an appropriate way. Provided that both f/V converters are identical, thermal effects on the pulse area are completely suppressed, but the low-frequency RMS noise is increased by a factor of $\sqrt{2}$. For the test circuit, we observed a reduction of the temperature-induced effects by about one order of magnitude.

The nonlinearity of the temperature-stabilized V/f converter was determined by applying a known voltage to its input using a Fluke 5720A calibrator combined with a Fluke 8508A voltmeter and by measuring the output frequency with an HP53132A counter. A gate time of 3 s was chosen, which results in sufficiently stable frequency readings. We observed short-term fluctuations of typically ± 1 Hz, and a drift of about 2 Hz during the complete measurement, which took 45 min.
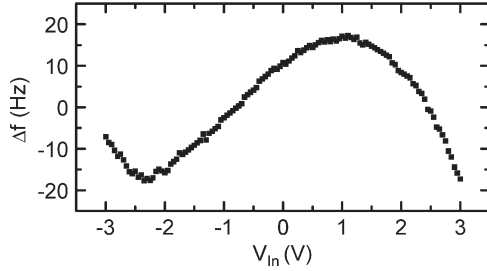
Fig. 7. Measured nonlinearity of the V/f converter test circuit over the input voltage range of ± 3 V. The output-frequency span is 1 MHz, centered around 1.5 MHz. The highest frequency of 2 MHz is obtained for $V_{\mathrm{In}} = -3$ V.

Fig. 8. Bridge-voltage difference $\Delta V_{\mathrm{Bridge}}$ versus cycle duration t_{Cycle} in a QHE vs. 100-Ω comparison. The error bars denote the expanded type A uncertainty. (Dotted line) Expected dependence estimated from the measured settling behavior of the bridge voltage [4].

Fig. 7 shows the obtained nonlinearity (maximum deviation from a linear fit) of ± 20 Hz, which corresponds to $\pm 2 \times 10^{-5}$ of the FS output or an integral nonlinearity of ± 1.3 least significant bits of an equivalent 16-bit analog-to-digital (A/D) converter. We expect that the remaining nonlinearity, as well as the low-frequency noise and thermal stability, can be further improved at the expense of a reduced bandwidth by lowering the output-frequency range (center frequency and span) and lengthening the pulse duration in the f/V converter correspondingly. Our circuit design allows such a downscaling by simply increasing the relevant capacitances accordingly.

The presented V/f converter provides an optical isolation of analog voltages with a high bandwidth, a good precision, and a relatively low noise level. For this, the optical output is back converted into an analog voltage with a f/V converter identical to the one in the servo loop. Systematic nonlinearities in both f/V converters are suppressed. Alternatively, the V/f converter may be used to digitize the nanovoltmeter output by using a counter instead of performing an analog back conversion. This scheme of the A/D conversion is monotonic and free of missing codes. It also integrates noise. Due to the high output frequency, a good resolution can be achieved in a short time. The power-line interference can be easily suppressed by selecting a counter gate time of integer multiples of one power-line cycle.

VI. APPLICATION EXAMPLES

Here, two application examples for the chopper amplifier are presented. The amplifier was primarily developed for use as a null detector in our new CCC-based resistance bridge [3]. In a typical experiment, a 100-Ω standard resistor is compared against the quantum Hall effect (QHE) at the filling factor $i = 2 \, (R_{K-90}/2 \approx 12.9 \, \mathrm{k\Omega})$ [10]. Currents are passed through both resistors to produce nearly identical voltage drops of 0.5 V. The very small difference between these voltage drops (the bridge voltage V_{Bridge}) is measured using the chopper amplifier. A high overall gain of 120 dB is typically selected.

To suppress the effect of thermal drifts, the currents are periodically reversed. The difference $\Delta V_{\mathrm{Bridge}}$ between the bridge voltages for both polarities is a measure of the resistance ratio. Typically, the cycle duration t_{Cycle} (the total time for one positive plus one negative polarity) is much larger than 1 s. A short cycle duration is desirable to minimize drift effects caused, for example, by thermal electromotive forces (EMFs) or air-pressure dependences. On the other hand, settling effects
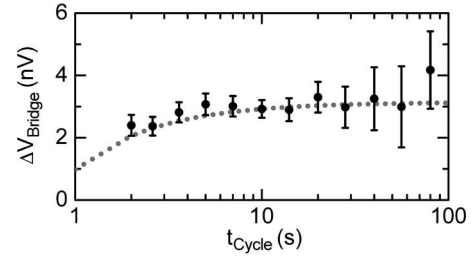
in the resistors and/or in the connecting cables after each current reversal set a lower limit for the cycle duration. The high speed of our chopper amplifier made it possible, for the first time, to investigate these effects over a wide range of cycle durations [4].

Fig. 8 shows the measured bridge-voltage difference $\Delta V_{\mathrm{Bridge}}$ as a function of the cycle duration for cable 2 in [4]. The bridge voltage was sensed by the chopper amplifier with a total measurement time of 24 min for each data point. Considering wait times after the current reversals, the net averaging time was 45% of the total measurement time. With cycle durations below about 10 s, a constant expanded type A uncertainty ($k = 2$; $\approx$95% confidence) of 0.32 nV is obtained, which corresponds to a statistical uncertainty in the resistance ratio of 3.2 parts in 10^{10}. As the averaging time is equal for all data points in Fig. 8, a constant type A uncertainty indicates the white noise. For long cycle durations $t_{\mathrm{Cycle}} > 10 \, \mathrm{s}$, the uncertainty increases due to the $1/f$ noise and the drift effects. This is however not caused by the chopper amplifier, which has a much better low-frequency noise performance (cf. Fig. 3). Rather, it is caused by parasitics in the experimental setup, e.g., thermal EMFs in the connecting cables and the resistor terminals or low-frequency excess noise in the cryogenic components (CCC and SQUID).

The chopper amplifier was also tested in an automated setup for the comparison of Josephson arrays [11]. The voltage step of one of the arrays was measured as a function of the bias current trim ΔI_{Bias}, whereas the other array was operated at its nominal working point. The microwave frequency was adjusted to obtain steps at 1.2 V. Like in the CCC experiment, the bias currents were reversed to suppress the drift effects. The voltage difference $\Delta V_{\mathrm{Array}}$ between the two arrays was determined from the readings obtained for the two current polarities. Fig. 9 shows $\Delta V_{\mathrm{Array}}$ measured with the chopper amplifier (black circles) and with an N11 nanovoltmeter (gray triangles). The complete sweeps from -1 to $+1$ mA in steps of 20 μA took about 2 h for the chopper amplifier and 3.5 h with the N11.

The chopper amplifier allows a precise measurement of the voltage step, whereas the N11 shows a large scattering in the displayed voltage values. This is not caused by a higher noise of the N11 because the voltage noise levels of both instruments are comparable, and current-noise effects do not play a role due to the low dynamic resistance of the arrays at the voltage step. Rather, the large scattering is a consequence of the too low measurement speed of the N11 in this automated setup, where the bias current is changed stepwise. During the current
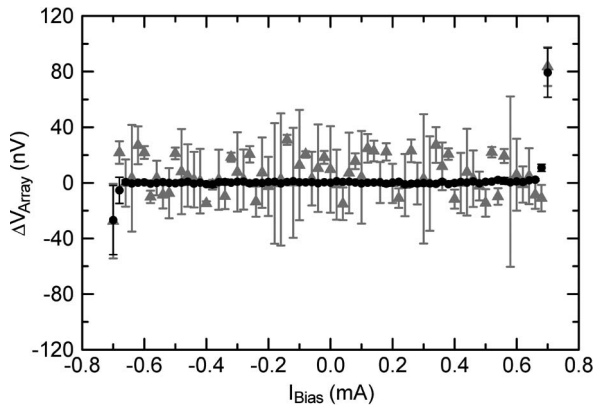
Fig. 9. Voltage difference ΔV_{Array} between two Josephson arrays versus the bias current variation ΔI_{Bias} in one array measured with an automated setup using (black circles) the chopper amplifier or (gray triangles) an N11 nanovoltmeter. Each data point is the result of one bias current cycle (positive and negative polarity). For the chopper amplifier, a wait time of 4 s after each polarity reversal was added before reading its output 40 times with an Agilent 3458A multimeter. The wait time after the polarity reversal for the N11 was 15 s (filter 1) before taking 30 readings. The error bars indicate the expanded type A uncertainty. Note that the bias current was changed stepwise, which heavily overloaded the N11 input during the current changes and resulted in substantially longer recovery times than that under normal operation conditions.

changes, the nanovoltmeter is heavily overloaded. The selected wait time of 15 s after each polarity reversal is not long enough for the N11 to fully recover (we also tried 30 s with no clear improvement). In contrast, for the chopper amplifier, the conservatively selected wait time of 4 s is by far sufficient (a recovery time below 0.2 s was observed in [3]). Note that the described measurements were mainly performed to evaluate the usefulness of the new chopper amplifier and of the quite common N11 for our existing setup designed for programmable Josephson array comparisons. The presented results mean neither that the N11 is not useful for the comparison of Josephson array voltage systems in general nor that the N11 is the best instrument from EM Electronics for this purpose. However, the superior performance of the new chopper amplifier in this unfavorable measurement setup (concerning overload requirements) clearly showed that it is a powerful and robust instrument for precision measurements. As a result, we decided to use two of the new amplifiers for our dual Josephson potentiometer [12].

VII. CONCLUSION

An ultralow-noise chopper amplifier has been presented, which combines dc precision with a high measurement bandwidth. Flexible postamplification and postfiltering circuitry, as well as a highly linear optical output, make the instrument well suited for many applications, e.g., as a nanovoltmeter in metrology or as a laboratory differential amplifier with a very high common-mode rejection. It is planned to make the amplifier commercially available in 2011 under license agreement [13].

ACKNOWLEDGMENT

REFERENCES

[1] [Online]. Available: http://www.emelectronics.co.uk/spec/N11.html
[2] D. Drung and J.-H. Storm, "Ultra-low noise chopper amplifier with low input charge injection," in *Proc. Dig. 27th Conf. Precision Electromagn. Meas.*, Daejeon, Korea, Jun. 2010, pp. 759–760.
[3] D. Drung, M. Götz, E. Pesel, J.-H. Storm, C. Amann, M. Peters, and T. Schurig, "Improving the stability of cryogenic current comparator setups," *Supercond. Sci. Technol.*, vol. 22, no. 11, p. 114 004, Nov. 2009.
[4] M. Götz, D. Drung, E. Pesel, and F.-J. Ahlers, "Settling behavior of the bridge voltage in resistance ratio measurements with cryogenic current comparators," *IEEE Trans. Instrum. Meas.*, 2011, submitted for publication.
[5] J. F. Witte, K. A. A. Makinwa, and J. H. Huijsing, *Dynamic Offset Compensated CMOS Amplifiers*. Dordrecht, The Netherlands: Springer-Verlag, 2009.
[6] B. P. Kibble and I. A. Robinson, "Guidance on eliminating interference from sensitive electrical circuits," NPL, Teddington, U.K., Report DES 129, 1993.
[7] J. R. Pickering, "High isolation power transformer," Patent WO 97/21 233, Jun. 12, 1997.
[8] T. J. Witt, "Using the Allan variance and power spectral density to characterize dc nanovoltmeters," *IEEE Trans. Instrum. Meas.*, vol. 50, no. 2, pp. 445–448, Apr. 2001.
[9] J. Beyer, "Transition-edge sensor series array bolometer," *Supercond. Sci. Technol.*, vol. 23, no. 10, pp. 105 019–105 025, Oct. 2010.
[10] J. Gallop and F. Piquemal, "SQUIDs for standards and metrology," in *The SQUID Handbook*, J. Clarke and A. I. Braginski, Eds. Weinheim, Germany: Wiley-VCH, 2006, pp. 95–137.
[11] L. Palafox, R. Behr, W. G. K. Ihlenfeld, F. Müller, E. Mohns, M. Seckelmann, and F. Ahlers, "The Josephson-effect-based primary AC power standard at the PTB: Progress report," *IEEE Trans. Instrum. Meas.*, vol. 58, no. 4, pp. 1049–1053, Apr. 2009.
[12] R. Behr, T. Funck, B. Schumacher, and P. Warnecke, "Measuring resistance standards in terms of the quantized Hall resistance with a dual Josephson voltage standard using SINIS Josephson arrays," *IEEE Trans. Instrum. Meas.*, vol. 52, no. 2, pp. 521–523, Apr. 2003.
[13] Magnicon GmbH, Hamburg, Germany. [Online]. Available: http://www.magnicon.com

Dietmar Drung was born in Mühlacker, Germany, in 1958. He received the Dipl.-Ing. and Dr.-Ing. degrees in electrical engineering from the University of Karlsruhe, Karlsruhe, Germany, in 1982 and 1988, respectively.

From 1983 to 1988, he was a Researcher with the University of Karlsruhe, where he worked on digital and analog circuits with Josephson junctions. Since 1988, he has been with the Physikalisch-Technische Bundesanstalt (PTB), Berlin, Germany, where he has been working on superconducting quantum interference devices (SQUIDs) and measurement systems for magnetic sensing and electrical metrology. He is currently a Senior Scientist in the field of superconducting sensors with the PTB. His activities include the development of high-speed direct-current SQUID readout electronics and low-noise amplifiers.

Jan-Hendrik Storm was born in Bad Oldesloe, Germany, in 1981. He received the Dipl.-Ing. (Fachhochschule) degree in applied physics from Brandenburg University of Applied Sciences, Brandenburg, Germany, in 2008.

Since 2008, he has been with the Physikalisch-Technische Bundesanstalt, Berlin, Germany, where he has been working on superconducting sensors and low-noise amplifiers.